Comparison of $PM_{2.5}$ carbonaceous pollutants between an urban site in Shanghai and a background island in Coastal East China Sea in summer: Concentration, Composition and Sources

Fengwen Wang[abc*], Tian Lin[d], Yuanyuan Li[b], Zhigang Guo[b], Neil L. Rose[e]

[a]State Key Laboratory of Coal Mine Disaster Dynamics and Control, Chongqing University, Chongqing 400030, China

[b]Shanghai Key Laboratory of Atmospheric Particle Pollution and Prevention (LAP^3), Fudan University, Shanghai 200433, China

[c]Department of Environmental Science, College of Resources and Environmental Science, Chongqing University, Chongqing 400030, China

[d]State Key Laboratory of Environmental Geochemistry, Institute of Geochemistry, Chinese Academy of Sciences, Guiyang 550002, China

[e]Environmental Change Research Centre, University College London, Gower Street, London WC1E 6BT, United Kingdom

[*]Corresponding author: fengwenwang@cqu.edu.cn

Abstract:

Nine paired samples of atmospheric particulate matter with an aerodynamic diameter less than or equal to 2.5 μm ($PM_{2.5}$) were collected concurrently at an urban site in Shanghai, China and a background site at Huaniao Island (HNI) in the coastal East China Sea (ECS) between July 21 and 29, 2011. The samples were analyzed for the 16 United States Environmental Protection Agency (USEPA) priority polycyclic aromatic hydrocarbons (PAHs), *n*-alkanes (20 species, C_{14}–C_{33}), hopanes (10 species,

C_{29}–C_{32}), and steranes (12 species, C_{27}–C_{29}). These two sites, approximately 66 km apart, are both on the pathway of land-based pollutants as they are transported to the ECS by seasonal winds. As expected, concentrations in Shanghai were higher (average: 8.4 and 67.8 ng/m^3 for 16 PAHs and *n*-alkanes, respectively) than those at HNI (average: 1.8 and 8.5 ng/m^3, respectively). The dominant contributor to 16 PAHs in Shanghai was 5–6-ring PAHs (60.0%), whereas 2–3-ring PAHs contributed the most (72.5%) at HNI. Plant waxes contributed 45.7% and 25.9% of the *n*-alkanes in Shanghai and HNI, respectively, implying a relatively greater contribution from petroleum residues to the *n*-alkanes at HNI. Principal component analysis (PCA) and the compositions of hopanes and steranes highlighted a prominent contribution from traffic emissions to carbonaceous $PM_{2.5}$ aerosols. This study provides comprehensive details about the sources, formation, and transport of pollutants from eastern China to the coastal ECS.

Keywords: Carbonaceous pollutants; $PM_{2.5}$; Shanghai; East China Sea; Sources

1 Introduction

Carbonaceous pollutants are a complex mixture of substances that represent a large, but highly variable fraction of the mass of particulate matter with an aerodynamic diameter less than or equal to 2.5 μm ($PM_{2.5}$) (i.e., usually 20–50%)[1]. They can be formed by a variety of processes that may be divided into two source categories: natural origins and anthropogenic combustion. Natural origins include wild fires, volcanic eruptions, and natural dust transport, whereas fossil-fuel combustion, vehicle exhaust, and biomass burning are the main anthropogenic origins[2-4]. Due to the importance of carbonaceous pollutants to aerosol sources as well as their detrimental effects on human

health and climate, many studies of their formation and transportation processes have been undertaken in urban, suburban, and remote environments worldwide[5-7].

The concentrations, compositions, and sources of these pollutants have also been foci of researchers. For example, Feng et al., (2007) reported the carbonaceous pollutant composition of $PM_{2.5}$ in Changdao, a resort island located between the Bohai Sea and the Yellow Sea in northern China, and apportioned sources based on a component analysis of specific molecular markers[8]. Cao et al. (2013) investigated the occurrence and compositions of carbonaceous pollutants (i.e., 24 *n*-alkanes and 17 polycyclic aromatic hydrocarbons: PAHs) on $PM_{2.5}$ and total suspended particulates (TSP) collected at a Shanghai suburban site and provided new ways to apportion their sources[9]. Chen et al. (2014) measured the compositions and sources of *n*-alkanes and PAHs in TSP from the southeastern Tibetan Plateau and found a prominent contribution from biomass burning transported from South Asia and western China, whereas Kunwar et al., (2014) reported 1-year observations of carbonaceous pollutants in TSP collected at Cape Hedo, Okinawa and discussed seasonal changes in the components and their transformation during transport[10,11]. These studies have highlighted the spatial and temporal variability in the concentration, composition, and sources of carbonaceous pollutants and have also shown that high-resolution studies, rather than low-resolution, regional assessments, are required to provide insight into the formation and transport mechanisms of these substances.

Shanghai, one of the largest (~24 million population in 2015) and most developed (~2 trillion yuan GDP in 2015) Chinese mainland cities, is located at the eastern end of

the Yangtze River Delta (YRD) and is bordered to the east by the East China Sea (ECS). The city is located in the transport pathway of continental pollutants flowing from mainland China to the ECS, which are driven by the East Asian monsoon[12,13]. The unique circulation pattern of this region has made the ECS a "receptor" of pollutants transported both from YRD (i.e., Shanghai) and adjacent regions, as demonstrated by recent, intensive aerosol pollution studies conducted at a remote site, Huaniao Island (HNI), in the coastal ECS[14-17]. These studies, however, were limited as data were collected only on the island, which did not allow comparison with other sites along the pollutant transport pathway. In this study, nine paired $PM_{2.5}$ samples were collected concurrently at an urban site in Shanghai, China and at HNI in the coastal ECS. These samples were analyzed for typical carbonaceous pollutants, including the 16 United States Environmental Protection Agency (USEPA) priority PAHs, 20 *n*-alkanes (C_{14}–C_{33}), hopanes (10 species), and steranes (12 species), with an emphasis on their concentrations, compositions, and sources. The aim of this study was to compare data on the pollution characteristics of carbonaceous aerosols at these paired sites, thereby directly contributing to a better understanding of pollutant transport from Shanghai and, possibly, the YRD to the coastal ECS.

2 Materials and Methods

2.1 Sampling sites and sample collection

The sampling site in Shanghai (31.3º N, 121.5º E) was at the top of a building at Fudan University[18]. With four floors, the building is roughly 20 m above ground and approximately 2 km from Wu-Jiao-Chang shopping center, one of the five sub-centers

in urban Shanghai. As this area is the site of faculty housing and a student dormitory, which is located to the south of the building, it is representative of both residential and commercial areas (Fig. 1). As a consequence, it has been used by researchers in many previous studies[19-22].

The sampling site in the ECS was positioned on the roof of a three-story building located at the northeast corner of HNI (N30.86˚, E122.67˚) (Fig. 1). This building is a small part of a state-owned lighthouse, with a building area of approximately 500 m^2. The sampling apparatus was placed at the center of the roof at a horizontal distance of 50 m from a fence and an elevation of ~50 m above sea level. HNI is 66 km from the east of Shanghai and has a land area of approximately 3.3 km^2 and a population of fewer than 1,000. The northeast part of the island is primarily covered by bare rocks, with some annual herb plants and windflowers. There is almost no industrial activity on the island. Most of the inhabitants reside in the southwest and subsist by fishing, making it an ideal site to compare the pollution characteristics of atmospheric organic pollutants in inland locations.

To concurrently collect $PM_{2.5}$ samples at both Shanghai and HNI, two identical $PM_{2.5}$ samplers (ASM-1, Guangzhou Mingye Huanbao Technology Company, Guangzhou, China) with a flow rate of 300 L min^{-1} were used. The $PM_{2.5}$ samples were collected on quartz filters (20×25 cm^2, T2600, Pall Corporation, Port Washington, NY, USA). The sampling time was 23.5 hours, starting at 09:00 and ending at 08:30 the following day. The sampling period was July 21–29, 2011, resulting in nine paired samples. This included periods when air masses were arriving at both Shanghai and

HNI from both continental and oceanic sources (see section 2.5). Two parallel operational sample blanks (i.e., field blanks) were obtained for each site. The sample blanks were obtained by placing filters into the sampler without pumping air; they were then immediately removed. The blanks were also analyzed for PAHs, *n*-alkanes, hopanes, and steranes to identify any possible contamination in the field. Before sampling, the quartz filters were wrapped in aluminum foil and combusted at 450°C for 4 h. After baking, the filters were sealed in marked valve bags and stored in a cool and dry location until they were prepared for sample collection. The sampled filters were preserved at -20°C prior to analysis.

2.2 Sample analysis for PAHs and *n*-alkanes

The sampling filter was firstly divided into two same half parts. The half part was then Soxhlet extracted for 48 hours with dichloromethane (DCM). The DCM was spiked with a known PAHs standard sample that was consisted of deuterated naphthalene (Nap-d_8, m/z 136) (200 ng), deuterated acenaphthene (Ace-d_{10}, m/z 164) (200 ng), deuterated phenanthrene (Phe-d_{10}, m/z 188) (200 ng), deuterated chryene (Chr-d_{12}, m/z 240) (200 ng) and deuterated perylene (Per-$_{12}$, m/z 264) (200 ng). These deuterated standard samples were used to monitor the efficiency (i.e., recovery rate) of the extracting process in lab.

After Soxhlet extraction, the extracts were moved into a vacuum rotary evaporator and rotary evaporated to about 5 mL at 40°C and 50 rpm/min. The samples were then transferred into 22 ml glass tubes and continued to concentrate to about 2 ml by N_2 (purity: 99%). The concentrates were then cleaned and fractionated on chromatography

alumina/silica columns (8 mm in diameter, 20 cm in length). From down to top, the columns were filled with 3 cm deactivated Al_2O_3 (1.53 g; mesh size: 100-200; supplier: Shanghai Guoyao Company), 3 cm SiO_2 (1.20 g, mesh size: 80-100; supplier: Jiangsu Qiangsheng Chemical Company) and 1 cm Na_2SO_4 (analysis grade; supplier: Shanghai Dahe Chemical Company). The columns were then eluted at least twice with 20 mL dichloromethane/hexane (1:1, v:v). The solvent was then exchanged for hexane and rotary evaporation continued until the sample was approximately 5 ml. Prior to PAH analysis, the extracts were further reduced to about 500 μL under N_2.

The 16 PAHs were: 2-ring: naphthalene (Nap); 3-ring: acenaphthylene (Ac), acenaphthene (Ace), fluorene (Fl), phenanthrene (Phe), anthracene (Ant); 4-ring: fluoranthene (Flu), pyrene (Pyr), benzo[a]anthracene (BaA), chrysene (Chr); 5-ring: benzo[b]fluoranthene (BbF), benzo[k]fluoranthene (BkF), benzo[a]pyrene (BaP), dibenzo[a,h]anthracene (DBA); 6-ring: indeno[1,2,3-cd]pyrene (IP), benzo[ghi]perylene (BghiP). The *n*-alkane was $C_{14}H_{30}$, $C_{15}H_{32}$, $C_{16}H_{34}$, $C_{17}H_{36}$, $C_{18}H_{38}$, $C_{19}H_{40}$, $C_{20}H_{42}$, $C_{21}H_{44}$, $C_{22}H_{46}$, $C_{23}H_{48}$, $C_{24}H_{50}$, $C_{25}H_{52}$, $C_{26}H_{54}$, $C_{27}H_{56}$, $C_{28}H_{58}$, $C_{29}H_{60}$, $C_{30}H_{62}$, $C_{31}H_{64}$, $C_{32}H_{66}$, $C_{33}H_{68}$.

The samples were injected with a certain amount of hexamethylbenzene (200 ng) for GC-MS analysis. The GC-MSD, namely Agilent GC 6890 N coupled with 5975C MSD, was equipped with DB5-MS column (30 m × 0.25 mm × 0.25 μm) and highly purified helium (99% in purity). The oven temperature was firstly set at 60°C for 2 min, then ramped to 290°C at 3 °C/min and held for 20 min. The injection temperature was at 290°C with an injection of split-less mode of the sample. The volume of the sample

was 1 μL with a 5 minutes delay of the solvent.

The concentration of PAHs and *n*-alkanes was determined by using authentic standards of the 16 PAHs (Nap, Ac, Ace, Fl, Phe, Ant, Flu, Pyr, BaA, Chr, BbF, BkF, BaP, DBA, IP, BghiP) and 10 even numbered *n*-alkanes (C_{14}, C_{16}, C_{18}, C_{20}, C_{22}, C_{24}, C_{26}, C_{28}, C_{30} and C_{32}), respectively. PAHs were quantified, for example, by the ions of m/z 128 for Nap, 178 for Phe and 252 for BbF, BkF, BaP. N-alkanes were quantified by the ions at m/z 57 and 71. The species identification was based on the mass spectra and retention times of the chromatographic peaks with those of authentic standards.

2.3 Sample analysis for hopanes and steranes

The extraction procedure and GC-MS analysis for hopanes and steranes was the same as for PAHs and *n*-alkanes. The hopanes and steranes were identified by monitoring the respective typical ions: m/z 191 for hopanes and m/z 217 for 5α-, 14α- and 17α-steranes and m/z 218 for 5α-, 14β- and 17β-steranes[23]. The targeted 10 hopanes and 12 steranes were displayed in Table S1 of supporting information. In this study, we could only present the relative abundances of hopanes and steranes rather than the concentration data without of the authentic reference standards.

2.4 Quality Assurance / Quality Control (QA/QC)

The dichloromethane (DCM) and hexane extracting the PAHs, *n*-alkanes, hopanes and steranes were both at HPLC grade (95% in purity) and were purchased from Shanghai ANPEL Scientific Instrument Company (www.anpel.com.cn). The vessels used in the experiment were all rinsed with hot potassium dichromate-sulfuric acid solution and left overnight. Then they were washed using de-ionized water (18.2 MΩ

Milli-Q) and wrapped in aluminum foil. Before sealing the vessels in marked valve bag, they were baked at 450°C for 4 hours in a muffle furnace to avoid the background contamination. All vessels were rinsed at least twice with reagents when using in lab.

The authentic reference standards of PAHs and *n*-alkanes were purchased from Accu Standard, Inc. (www.accustandard.com). The extracting efficiency for *n*-alkanes was based on recovery rate of Phe-d_{10} and Chr-d_{12} as they were suggested to indicate recovery rate of the targeted *n*-alkanes[24]. The average recovery rates were 90±14% for Phe-d_{10} and 103±15% for Chr-d_{12}. The detection limits for 16 PAHs was from 0.008 to 0.08 ng/m^3; while for 20 *n*-alkanes, they were from 0.01 to 0.1 ng/m^3 [4]. Blank filters were analyzed to determine any background contamination and they showed no detectable carbonaceous pollutants. Procedural blanks and standard-spiked blanks were performed to monitor procedural performance and matrix effects. The concentrations reported here were not corrected for recovery efficiency.

2.5 Air mass back trajectory

The use of air mass back trajectories is a common way to trace atmospheric transport pathways and an altitude of 700 m has been used previously to trace long-range air mass transport at HNI[14]. In this study, 3-day back trajectories from Shanghai and HNI at 1200 UTC were calculated at both 100 m (local) and 700 m (long-range) above ground level at 12-hour intervals for all sampling days. The trajectory database was originated from HYSPLIT Trajectory Model on NOAA website. The downloaded datasets were then integrated using PC-based HYSPLIT Trajectory Model software. Detailed applications of the model on atmospheric transport and dispersion have been

described by Draxler, R.R., et al., (1997, 1998, 1999)[25-27]and Stein, A.F., et al., (2015)[28] as showed on "www.arl.noaa.gov/HYSPLIT_pubs.php".

3 Results and discussion

3.1 Air mass back trajectory conditions

Three-day back trajectories from altitudes of both 100 m (Fig. 2A) and 700 m (Fig. 2B) arriving at Shanghai (red lines) and HNI (blue lines) during the 9-day sampling period are shown in Fig. 2. For the 100-m altitude trajectory, the air parcels arriving at the two sites were almost the same and were comprised of three parts: derived from southern coastal regions and the open eastern and northern seas. For the 700-m altitude trajectory, the air parcels at the two sites were also quite similar, with half derived from the east (open sea) and half from the YRD region (continental). During sampling, the atmospheres of both sampling locations were influenced by source regions from around the YRD (contaminated) and air transport from the open sea (clean). However, there were also some obvious differences. Compared with that derived from HNI, the YRD-derived air mass arriving at Shanghai originated from farther southwest (i.e., southern China) and, therefore, was a source of more anthropogenic pollutants (i.e., industrial emissions, vehicle exhaust, etc.). The concentrations of PAHs and *n*-alkanes in Shanghai were much higher than those in HNI, but no obvious corresponding relationship (high to high/ low to low levels) could be found for each paired sample (see Table 1 in the following section). This indicates that not only the air mass transport path but also other factors, such as meteorological conditions and emission sources, played important roles in the concentrations of PAHs and *n*-alkanes. This will be further

discussed in the next section.

3.2 Concentrations of PAHs and *n*-alkanes

The concentrations of the 16 PAHs and 20 *n*-alkanes in $PM_{2.5}$ during the sampling period are presented in Table 1 along with several statistical indices, including the average ± standard deviation (stdev), median, and percentiles (5–95%). The concentrations of individual PAHs and *n*-alkanes in all $PM_{2.5}$ samples are shown in Table S2 of supporting information. The concentrations of 16 PAHs (ng/m^3) in Shanghai (range: 6.0–11.8; average ± stdev: 8.4 ± 2.3) were more than four times higher than those at HNI (range: 1.5–2.4; average ± stdev: 1.8 ± 0.3). The concentration differences between the two sites for 20 *n*-alkanes (ng/m^3) were similar to those of the 16 PAHs, ranging from 34.8 to 147.3 for Shanghai (average ± stdev: 67.8 ± 36.0) and from 3.3 to 23.4 for HNI (average ± stdev: 8.5 ± 6.9). The higher concentrations of PAH and *n*-alkanes in Shanghai compared with HNI were consistent with the air mass transport pathway described above, indicating a relatively severe fine particulate pollution and multi-anthropogenic source contribution to airborne particles in Shanghai.

Table 2 provides a comparison of the PAH and *n*-alkane concentrations in the paired samples with those from other studies worldwide. The PAH and *n*-alkane concentrations in Shanghai and at HNI in summer 2011 were comparable to those in 2012[15-18] as well as to those reported in a paired study of TSP undertaken in the USA at an urban site in Chicago and a remote location at Lake Michigan[29]. Compared with a study of TSP undertaken at the Liberty Science Center in New Jersey and Raritan Bay, which is adjacent to Staten Island[30], the concentrations of *n*-alkanes at Shanghai and

HNI were much higher, although concentrations of PAHs were more comparable[9,19,31,32]. The concentrations of PAHs at HNI were comparable to those reported in remote regions of Europe[33,34] and Tibet[10], but the *n*-alkane concentrations were higher. Table 2 also summarizes the concentrations of particulate PAHs in Shanghai in 2003, 2006, 2009, 2011, 2012, and 2015. It was found that the PAH concentrations in $PM_{2.5}$ in the summer in Shanghai were relatively stable over the past 10 years. The PAH concentration in summer was the lowest of all four seasons[18]. Previous studies have suggested that the reasons for the stable concentrations were the similar meteorological conditions and the influence of air mass transport pathways[19,31]. When compared with the other seasons, the frequency of sunny days in summer was higher and solar radiation was more intense, resulting in more rapid photochemical degradation of PAHs[35]. In summer, the prevailing winds in Shanghai are mostly from relatively "clean" open sea, acting as a significant "dilution" of "local-emitted" PAHs at any time[18].

3.3 Compositions of PAHs and *n*-alkanes

The composition of PAHs and *n*-alkanes during the sampling period is plotted in Fig. 3 and reflects a distinctly different pattern in the overall composition of the PAHs in all samples from the two sites. For Shanghai, 5~6-ring PAHs (BbF, BkF, BaA, DBA, IP, and BghiP) contributed most to the total PAHs (60.0%), with 4-ring PAHs (Flu, Pyr, BaA, and Chr) ranked second (22.7%), followed by 2~3-ring PAHs (Nap, Ac, Ace, Fl, Phe, and Ant) (17.3%). In contrast, at HNI, 2~3-ring PAHs contributed the most to the total PAHs (72.5%), followed by 4-ring PAHs (19.6%) and 5~6-ring PAHs (7.9%). The 5~6-ring PAHs, such as BkF, BaP, and BghiP, are indicators of diesel vehicle and

gasoline emissions[36], whereas 2~3-ring PAHs, such as Nap, Ace, FL, and Phe, are more abundant in natural mineral dust[37]. These composition patterns are similar to those reported in our previous study, which also found major contributions from 5~6-ring PAHs in Shanghai (56.5%) and 2~3-ring PAHs at HNI (55.6%)[15].

The compositions of *n*-alkanes in Shanghai and HNI were similar for low carbon number (C_{14}–C_{23}) compounds, but there were clear differences for the high carbon-number *n*-alkanes (C_{24}–C_{33}). An odd-to-even dominance among the C_{24}–C_{33} *n*-alkanes was observed in Shanghai, whereas the concentrations of odd and even *n*-alkanes were almost equal at HNI. The carbon preference index (CPI) of *n*-alkanes has been used to characterize the biogenic and anthropogenic origins of materials[38]. In this study, the CPI = $\sum(C_{15}–C_{33})/\sum(C_{14}–C_{32})$, which was calculated as the sum of the concentrations of the odd carbon-number *n*-alkanes divided by the sum of the concentration of the even carbon-number *n*-alkanes. The CPI averaged 1.7 for Shanghai and 1.2 for HNI (Table 1). A CPI of ~1.0 indicates anthropogenic sources (e.g., petroleum residues and gasoline emissions)[38] and, therefore, the higher CPI for Shanghai compared with HNI indicated a reduced contribution from anthropogenic sources to those with a biogenic origin.

3.4 Source categories of PAHs and *n*-alkanes

As shown in Fig. 4, the diagnostic ratios used to determine the source categories in this study were Phe/(Phe+Ant), Flu/(Flu+Pyr), BaA/(BaA+Chr), and IP/(IP+BghiP). The ratio of Phe/(Phe+Ant) was 0.89 for Shanghai and 0.93 for HNI, suggesting that the dominant source of these PAHs was coal combustion and biomass burning[33]. The ratios of Flu/(Flu+Pyr) for Shanghai and HNI were both >0.5, indicating a dominant

contribution from the combustion of coal, wood, and grass. The values of BaA/(BaA+Chr) were 0.37 for Shanghai and 0.50 for HNI, both indicating vehicular emission[29]. There was almost no difference in the ratios of IP/(IP+BghiP) for the two sites (0.60 and 0.55, respectively), also implying a contribution from the combustion of coal, wood, and grass[39]. These results suggest that the $PM_{2.5}$-bound PAHs arriving at the two sites probably have common sources, such as the combustion of coal, wood, and grass, as well as vehicular emissions.

According to Simoneit et al. (1991)[40], *n*-alkanes can be divided into two source categories: plant waxes and petroleum residues. In this study, C_{max} (the *n*-alkane with the highest concentration) was C_{29} or C_{31}, suggesting a predominance of biogenic sources, especially epicuticular waxes from higher plants. The contribution of plant wax-derived *n*-alkanes can be calculated from the following equation: Wax $C_n = [C_n-(C_{n+1}+C_{n-1})/2]/C_n$, with the contributions for all 18 samples at the two sites listed in Table 1. The contribution of wax-derived *n*-alkanes to the totals in Shanghai and HNI were 45.7 and 25.9%, respectively. The sampling site in Shanghai was on the roof of a campus building, which was surrounded by the green belt of the campus; the site in HNI was mostly covered by bare rocks and was potentially influenced by ship emissions associated with two busy ports, Yangshan Port and the Port of Shanghai[18]. Therefore, the higher contributions from plant-wax in Shanghai compared with HNI may be due to processes such as the abrasion of leaves and pollen from trees around the sampling site. These percentages are comparable to those reported for summer 2012 in Shanghai (plant wax-*n*-alkanes = 49.8%)[4] but are higher than those reported for HNI

(plant wax-*n*-alkanes = 9.0%)[16]. Feng et al. (2006)[19] used the same method and sampling site in Shanghai and estimated that about 20% of the *n*-alkanes in summer (n = 7) were from biogenic sources, which was only about half the amount found in this study (45.7%). The differences between these studies suggest temporal variations at sampling sites and uncertainties associated with the sample number and sampling apparatus.

3.5 Source identification of selected PAHs (eight species) and *n*-alkanes (eight species) using principal component analysis (PCA)

PCA using SPSS 16.0 (SPSS Inc., Chicago, IL, USA) was performed on datasets containing eight PAHs (Phe, Ant, Flu, Pyr, BaA, Chr, IP, and BghiP) and eight *n*-alkanes ($C_{14}H_{30}$, $C_{15}H_{32}$, $C_{22}H_{46}$, $C_{23}H_{48}$, $C_{28}H_{58}$, $C_{29}H_{60}$, $C_{30}H_{62}$, and $C_{31}H_{64}$). The eight PAHs were the "diagnostic ratio" species referred to in section 3.4, and the eight *n*-alkanes were representative of low, middle, and high carbon number *n*-alkanes. Two PCs, PC1 and PC2, were extracted and are shown in Table 3. For PAHs, the PCs explained 82.4% (63.1 and 19.3%, respectively) of the total variance for Shanghai and 86.1% (49.8 and 36.3%, respectively) for HNI. For *n*-alkanes, the PCs explained 94.5% (86.8 and 7.7%, respectively) of the total variance for Shanghai and 94.5% (70.0 and 24.5%, respectively) for HNI. The four biplots with PC scores and loadings of eight PAHs and n-alkanes in $PM_{2.5}$ collected at Shanghai and HNI using correlation matrix are shown in Figure S1-S4 of supporting information.

For PAHs, PC1 of both Shanghai and HNI had high loadings of BaA, Chr, IP, and BghiP, whereas PC2 of Shanghai was dominated by Phe and Ant and PC2 of HNI was

more evidently characterized by Phe, Flu and Pyr. Therefore, PC1 of the two sites were primarily associated with vehicular emissions[15], PC2 of Shanghai was associated with coal combustion[36], and PC2 of HNI was most likely associated with biomass burning[2]. Because there was a higher loading of PC1 in Shanghai (63.1%) than HNI (49.8%), it was concluded that vehicular emissions had more influence on PAH emissions in Shanghai than in HNI during the sampling period.

For *n*-alkanes, PC1 of both Shanghai and HNI had high loadings of $C_{23}H_{48}$, $C_{28}H_{58}$, $C_{29}H_{60}$, $C_{30}H_{62}$, and $C_{31}H_{64}$. PC2 of Shanghai was solely dominated by $C_{22}H_{46,}$ whereas PC2 of HNI had a high loading of $C_{14}H_{30}$ and $C_{15}H_{32}$. C_{26}–C_{33} *n*-alkanes are typical markers of biogenic sources, whereas C_{14}–C_{19} mainly originates from petroleum residue. Therefore, the PC1 of these two sites were considered to be associated with biogenic sources, and PC2 represented a petroleum residue source. A higher factor contribution from PC1 in Shanghai (86.8%) compared with HNI (70.0%) indicated more prominent biogenic sources of *n*-alkanes in $PM_{2.5}$ in Shanghai during the sampling period.

3.6 Relative abundances of hopanes, steranes, and source implications

Table 1 shows the concentration ratios of Ts/Tm, αβC31 S/(S+R), and αααC29 S/(S+R) in all samples. The Ts/Tm ranged from 0.52 to 0.76 for Shanghai and 0.74 to 0.94 for HNI, with average values of 0.66 ± 0.07 and 0.82 ± 0.09, respectively. The αβC31 S/S+R ranged from 0.51 to 0.65 for Shanghai and 0.52 to 0.62 for HNI, with average values of 0.56 ± 0.04 and 0.58 ± 0.04, respectively. In terms of αααC29 S/(S+R), the ratios ranged from 0.46 to 0.60 for Shanghai and 0.43 to 0.56 for HNI, with each

having the same mean value of 0.52±0.05. As suggested by Feng et al. (2005)[41], a lower Ts/Tm indicates an enhanced impact from the combustion of less thermally maturated fossil fuels, such as biomass and coal combustion. Further evidence for a fossil-fuel input is determined by the ratio of αβC31S/(S + R), both approaching 0.6, indicating a major contribution from traffic emissions[42]. However, the value of αααC29 S/(S+R) was close to 0.5, indicating fully mature petroleum residues[43] and suggesting an origin from petroleum products contaminating the atmosphere of Shanghai and HNI[44].

Fig. 5 shows the distribution of hopane (10 species) and sterane (12 species) abundances relative to 18α(H)-22,29,30-trisnorneohopane (Ts: where Ts = 1) and C27-5α(H), 14α(H), 17α(H)-steranes (C27ααα(20S): where C27ααα(20S) = 1) measured in Shanghai and HNI, respectively. The distributions of hopanes in Shanghai and at HNI were quite similar, with the most abundant compounds being 17α(H) and 21β(H)-hopane (C30αβ), followed by 17α(H) and 21β(H)-norhopane (C29αβ). C30αβ is predominantly produced by wood burning[45], whereas C29αβ is a tracer for motor vehicle exhaust[46], providing evidence of contributions from these two sources. The pattern of steranes at both sites revealed the dominance of C29αββ(20R), followed by C29ααα(20S) and C29ααα(20R) (Fig. 5). The predominance of the C29 over the C28 and C27 steranes was also reported in surface sediments from the Sfax-Kerkennah coastal zone in Tunisia[41]and the Bohai Sea, China[23].

The compositions of hopanes and steranes combined with these characteristic ratios confirmed the contribution from biomass burning, traffic emissions, and petroleum to the $PM_{2.5}$ of Shanghai and HNI. Because there is almost no industrial

activity on HNI, the hopanes and steranes most likely originated from long-range atmospheric transport. With two large ports, the Port of Shanghai and Yangshan Port, the coastal ECS is busy, with activity from both public ferries and national and international cargo shipping. Shipping traffic in the coastal ECS is therefore the most likely source of the hopanes and steranes in the $PM_{2.5}$ of HNI. Detailed quantitative measurements for specific hopanes and steranes in aerosols at HNI, combined with size distribution and temporal data, are required to further investigate these sources.

4 Conclusions

A comprehensive study of the concentrations, compositions, and sources of carbonaceous pollutants in $PM_{2.5}$ was undertaken using paired samples from an urban site in Shanghai and an island location, HNI, in the coastal ECS during summer 2011. Shanghai, as expected, had relatively high levels of carbonaceous pollutants in comparison to HNI. The compositions of 16 PAHs and 20 *n*-alkanes for the two sites were significantly different, implying that the predominant sources were also distinctly different; however, the diagnostic ratios for PAHs suggested common sources, such as the combustion of coal, wood, and grass, and vehicular emissions. Plant waxes contributed more *n*-alkanes in Shanghai (average: 45.7%) than in HNI (average: 25.9%), probably due to biogenic activities, such as the abrasion of leaves and pollen transport. PCA confirmed a common dominant source from vehicular emissions for PAHs and a biogenic source for *n*-alkanes at the two sites. Vehicular exhaust emissions and shipping traffic were important contributors to the burden of hopanes and steranes in Shanghai and HNI, respectively.

Acknowledgement

This work was funded by the National Natural Science Foundation of China (NSFC) (No: 41603102, 21277030), the Opening Project of Shanghai Key Laboratory of Atmospheric Particle Pollution and Prevention (LAP^3) (No: FDLAP16007); and Hangzhou Research Project for Environmental Protection (No: 2012001). We would like to thank Mr. Chuanliang Ma and Miss Huaiyu Fu for the sample collection.

References

1 Cao, J. J., Lee, S. C., Ho, K. F., Zou, S. C., Fung, K., Li, Y., Watson, J. G., and Chow, J. C. *Atmos. Environ.*, 2004, 38, 4447-4456.

2 Rajput, P., Sarin, M.M., Rengarajan, R., Singh, D., *Atmos. Environ.*, 2011, 45, 6732-6740.

3 Kong, S.F., Ji, Y.Q., Li, Z.Y., Lu, B., Bai, Z.P., *Atmos. Environ.*, 201377, 155-165.

4 Wang, F.W., Guo, Z.G., Lin, T., Rose, N.L., *Chemosphere*, 2016, 146, 238-244.

5 Jacobson, M., *Nature*, 2001, 409, 695-697.

6 Barrett, T. E., Robinson, E. M., Usenko, S., Sheesley, R. J., *Environ. Sci. Technol.*, 2015, 49(19): 11631-11639.

7 Feng, J.L., Hu, J.C., Xu, B.H., Hu, X.L., Sun, P., Han, W.L., Gu, Z.P., Yu, X.M., Wu, M.H.,. *Atmos. Environ.*, 2015, 123, 288-297.

8 Feng, J.L., Guo, Z.G., Chan, C.K., Fang, M., *Atmos. Environ.*, 2007, 41, 1924-1935.

9 Cao, J. J. Zhu, C. S. Tie, X. X. Geng, F. H. Xu, H. M. Ho, S. S. H. Wang, G. H. Han, Y. M. Ho, K. F., *Atmos. Chem. Phys.*, 2013, 13(2):803-817.

10 Chen, Y., Cao, J.J., Zhao, J., Xu, H.M., Arimoto, R., Wang, G.H., Han, Y.M., Shen, Z.X., Li, G.H., *Sci. Total Environ.*, 2014, 470-471 (0):9-18.

11 Kunwar, B., Kawamura, K., *Atmos. Chem. Phys.*, 2014, 14(4): 1819-1836.

12 Zhang, K., Gao H.W., *Atmos. Environ.*, 2007, 41, 9136-9145.

13 Guo, L., Chen, Y., Wang, F. J., Meng, X., Xu, Z. F., Zhuang, G. S., *Mar. Chem.*, 2014, 163, 19-27.

14 Zhu, L., Chen, Y., Guo, L., Wang, F.J., *Atmos. Environ.*, 2013, 69, 131-138.

15 Wang, F.W., Lin, T., Li, Y.Y., Ji, T., Ma, C.L., Guo, Z.G., *Atmos. Environ*., 2014, 92, 484-492.

16 Wang, F.W., Guo, Z.G., Lin, T., Hu, L.M., Chen, Y.J., Zhu, Y.F., *Atmos. Environ.*, 2015, 110, 163-173.

17 Wang, F. J., Chen, Y., Meng, X., Fu, J. P., Wang, B., *Atmos. Environ.*, 2016, 127, 22-23.

18 Wang, F.W., Lin, T., Feng, J.L., Fu, H.Y., Guo, Z.G., *Environ. Sci. Processes. Impacts*, 2015, 17, 197-205.

19 Feng, J.L., Chan, C.K., Fang, M., Hu, M., He, L.Y., Tang, X.Y. *Chemosphere*. 2006, 64, 1393-1400.

20 Hou, B., Zhuang, G., Zhang, R., Liu, T., Guo, Z., Chen, Y., *J. Haz. Mater.*, 2011, 190, 529-536.

21 Huang, K., Zhuang, G., Lin, Y., Fu, J., Wang, Q., Liu, T., Zhang, R., Jiang, Y., Deng, C., Fu, Q., *Atmos. Chem. Phys.*, 2012, 12, 105-124.

22 Cheng, T.T.., Xu, C., Duan, J.Y., Wang, Y.F., Leng, C.P., Tao, J., Che, H.Z., He, Q.S., Wu, YF.., Zhang, R.J., Li, X., Chen, J.M., Kong, L.D.., Yu, X.N., *Atmos. Environ.*, 2015, 123, 315-326.

23 Hu, L., Guo, Z., Feng, J., Yang, Z., Fang, M., *Mar. Chem.*, 2009, 113, 197-211.

24 Guo, Z., Lin, T., Zhang, G., Hu, L., Zheng, M., *J. Hazard. Mater.*, 2009, 170, 888-894.

25 Draxler, R.R., G.D. Hess., *ERL ARL-224, NOAA Air Resources Laboratory, Silver Spring, MD,* 1997, 24 pp.

26 Draxler, R.R., G.D. Hess., *Aust. Meteor. Mag.,* 1998, 47, 295-308.

27 Draxler, R.R., *NOAA Tech. Memo. ERL ARL-230, NOAA Air Resources Laboratory, Silver Spring, MD,* 1999.

28 Stein, A.F., Draxler, R.R, Rolph, G.D., Stunder, B.J.B., Cohen, M.D., Ngan, F., *Bull. Amer. Meteor. Soc.*, 2015, 96, 2059-2077.

29 Simcik, M., Eisenreich, S., Lioy, P., *Atmos. Environ.*, 1999, 33, 5071-5079.

30 Gigliotti, C., Brunciak, P., Dachs, J., Glenn, I., Thomas, R., Nelson, E., Totten, L., Eisenreich, S., *Environ. Toxicol. Chem.*, 2002, 21, 235-244.

31 Chen, Y.J., Feng, Y.L., Xiong, S.C., Liu, D.Y., Wang, G., Sheng, G.Y., Fu, J.M., *Environ. Monit. Assess.*, 2011, 172(1): 235-247.

32 Wang, Q.Y., Kobayashi, K., Lu, S.L., Nakajima, D., Wang, W.Q., Zhang, W.C., Sekiguchi, K., Terasaki, M., *Environ. Pollut.*, 2016, 214, 149-160.

33 Fernández, P., Carrera, G., Grimalt, J.O., Ventura, M., Camarero, L., Catalan, J., *Environ. Sci. Technol.*, 2003, 37: 3261-3267.

34 Rissanen, T., Hyötyläinen, T., Kallio, M., Kronholm, J., Kulmala, M., Riekkola, M.L., *Chemosphere*, 2006, 64: 1185-195.

35 Castro, L., Pio, C., Harrison, R.M., Smith, D., *Atmos. Environ.*, 1999, 33, 2771-2781.

36 Harrison, R., Smith, D., Luhana, L., *Environ. Sci. Technol.*, 1996, 30, 825-832.

37 Moon, K.J., Han, J.S., Ghim, Y.S., Kim, Y.J., *Environ. Int.*, 2008, 34, 654-664.

38 Simoneit, B., *International Journal of Environ. Ana. Chem.*, 1986, 23, 207-237.

39 Yunker, M., Macdonald, R., Vingarzan, R., Mitchell, R., Goyette, D., Sylvestre, S., *Org. Geochem.*, 2002, 33, 489-515.

40 Simoneit, B., Sheng, G., Chen, X., Fu, J., Zhang, J., Xu, Y., *Atmos. Environ. Part A. General Topics*, 1991, 25, 2111-2129.

41 Feng, J., Chan, C., Fang, M., Hu, M., He, L., Tang, X., *Chemosphere*, 2005, 61, 623-632.

42 Fraser, M., Cass, G., Simoneit, B., *Environ. Sci. Technol.*, 1998, 32, 2051-2060.

43 Zaghden, H., Kallel, M., Elleuch, B., Oudot, J., Saliot, A., *Mar. Chem.*, 2007, 105, 70-89.

43 Aboul-Kassim, T.A.T., Simoneit, B.R.T., *Mar. Chem.*, 1996, 54, 135–158.

44 Moldowan, J.M., Albrecht, P., Philp, R.P., Biological markers in sediments and petroleum *Prentice Hall, Englewood Cliffs*, New Jersey, 1992， 156–181.

45 Standley, L.J., Simoneit, B.R.T., Environ. Sci. Technol., 1987, 21, 163-169.

46 Schauer, J., Kleeman, M., Cass, G., Simoneit, B., Environ. Sci. Technol., 2002, 36, 1169-1180.

Table captions

Table 1 Concentrations and some indices of carbonaceous pollutant in $PM_{2.5}$ from Shanghai and HNI. (n=9, for each site, " - " indicates not detected).

Table 2 Comparison of PAH and *n*-alkanes concentrations in $PM_{2.5}$ in this study with those from other studies worldwide.

Table 3 Correlation factor loading matrix of selected 8 PAHs and 8 *n*-alkanes in $PM_{2.5}$ collected at Shanghai and HNI. (" - " indicate values of the factor loading below zero)

Figure captions

Figure 1. Sampling sites at Shanghai and Huaniao Island (HNI).

Figure 2. 3-day back trajectories from both 100 m (A) and 700 m (B) altitude arriving at Shanghai and HNI. (The red and blue lines indicate air masses toward Shanghai and HNI sampling site, respectively.)

Figure 3. The compositions of PAHs and *n*-alkanes in $PM_{2.5}$ from Shanghai and HNI.

Figure 4 The diagnostic ratios of Phe/(Phe+Ant), Flu/(Flu+Pyr), BaA/(BaA+Chr) and IP/(IP+BghiP) of $PM_{2.5}$ at Shanghai and HNI.

Figure 5 Distribution diagrams of relative hopane and sterane abundances of $PM_{2.5}$ at Shanghai and HNI. (Ts:18α(H)-22,29,30-trisnorneohopane;Tm:17α(H)-22,29,30-trisnorhopane;C_{29}αβ:17α(H),21β(H)-norhopane;C_{29}βα:17β(H),21α(H)-norhopane;C_{30}αβ:17α(H),21β(H)-hopane;C_{30}βα:17β(H),21α(H)-hopane;C_{31}S:22S-17α(H),21β(H)-homohopane;C_{31}R:22R-17α(H),21β(H)-homohopane;C_{32}S:22S-17α(H),21β(H)-bishomohopane;C_{32}R:22R-17α(H),21β(H)-bishomohopane)

(C27ααα(20S), C27αββ(20R), C27αββ(20S), C27ααα(20R), C28ααα(20S), C28αββ(20R), C28αββ(20S), C28ααα(20R), C29ααα(20S), C29αββ(20R), C29αββ(20S), C29ααα(20R), and ααα

= 5α(H), 14α(H), 17α(H)-steranes; αββ = 5α(H), 14β(H), 17β(H)-steranes, R and S = C-20 R and S configuration, respectively.

Table 1 Concentrations and some indices of carbonaceous pollutant in $PM_{2.5}$ from Shanghai and HNI (n=9, respectively, " - " indicates not detected.).

Site	Date	16 PAHs	*n*-alkanes (C_{14}-C_{33})				hopanes		steranes
		ng/m^3	yield (ng/m^3)	CPI	C_{max}	waxed (%)	Ts/Tm	αβC31 S/(S+R)	ααα C29 S/(S+R)
Shanghai	7/21/2011	11.2	81.9	1.3	C_{29}	25.0	0.68	0.58	0.49
	7/22/2011	8.7	36.1	1.9	C_{29}	53.7	0.70	0.65	0.52
	7/23/2011	6.0	90.6	0.8	C_{24}	43.7	0.65	0.51	0.48
	7/24/2011	6.5	34.8	2.2	C_{31}	65.5	-	0.52	0.46
	7/25/2011	7.0	51.0	2.0	C_{29}	54.9	0.72	0.51	0.57
	7/26/2011	10.9	38.5	2.0	C_{29}	72.8	0.61	0.54	0.51
	7/27/2011	11.8	147.3	1.4	C_{29}	29.0	0.76	0.57	0.46
	7/28/2011	7.5	58.7	1.8	C_{29}	34.5	0.66	0.56	0.54
	7/29/2011	6.4	71.0	1.5	C_{29}	32.3	0.52	0.58	0.60
	Average	**8.4**	**67.8**	**1.7**	**C_{29}**	**45.7**	**0.66**	**0.56**	**0.52**
HNI	7/21/2011	1.8	16.7	1.1	C_{31}	29.3	0.74	0.59	0.52
	7/22/2011	1.9	23.4	1.0	C_{31}	42.2	0.91	0.62	0.52
	7/23/2011	2.4	4.8	1.1	C_{27}	24.9	0.79	0.57	0.56
	7/24/2011	1.8	4.7	1.1	C_{27}	16.5	0.94	0.59	0.54
	7/25/2011	2.0	6.3	1.2	C_{29}	28.2	-	0.58	0.54
	7/26/2011	1.7	6.6	1.2	C_{29}	26.2	-	0.58	0.43
	7/27/2011	1.5	6.8	1.2	C_{29}	24.0	-	0.52	-
	7/28/2011	2.0	4.3	1.3	C_{31}	26.4	-	0.52	0.54
	7/29/2011	1.6	3.3	1.1	C_{26}	24.9	0.75	0.61	0.51
	Average	**1.8**	**8.5**	**1.2**	**C_{29}**	**26.9**	**0.82**	**0.58**	**0.52**

Table 2 Comparison of PAH and *n*-alkanes concentrations in $PM_{2.5}$ in this study with other studies measured worldwide.

Site	Time	Sample number	Type	PAHs	PAHs summed	*n*-alkanes	References
Shanghai	2011,07	n=9	$PM_{2.5}$	8.4	16	67.8	This study
HNI		n=9	$PM_{2.5}$	1.8	16	8.6	
Shanghai	2012,07-08	n=18	$PM_{2.5}$	6.4	16	57.8	Wang et al., (2015b,2016b)
HNI		n=14	$PM_{2.5}$	1.0	16	13.4	Wang et al., (2014,2015a)
Chicago	1994-1995	n=73	TSP	45	26	-	Simcik et al., (1999)
Lake Michigan		n=73	TSP	2.9	26	-	
New Jersey	1998,07	n=12	TSP	2.9	26	-	Gigliotti et al., (2002)
Raritan Bay		n=3	TSP	0.8	26	-	
Shanghai	2015,08	n=7	$PM_{3.3}$	7.3	26	-	Wang et al., (2016c)
Shanghai	2009,09	n=20	$PM_{2.5}$	7.2	17	32.2 (C_{17}-C_{40})	Cao et al., (2013)
Shanghai	2006,07	n=28	TSP	17.9	17	-	Chen et al., (2011)
Shanghai	2003,08	n=7	$PM_{2.5}$	7.1	16	22.5 (C_{17}-C_{36})	Feng et al., (2006)

Table 3 Varimax rotated factor loading matrix of 15PAHs (DBA excluded) and 20 *n*-alkanes (C_{14}-C_{33}) in $PM_{2.5}$ collected at SH and HNI. (Middle and high values of the factor loading are boldfaced.)

$PM_{2.5}$ (2011,summer)	Shanghai			HNI		
	PC1	PC2	PC3	PC1	PC2	PC3
Nap	0.07	-	**0.62**	-	0.29	0.13
Ac	-	0.37	**0.70**	-	0.28	**0.69**
Ace	-	-	**0.93**	0.08	0.11	**0.68**
Fl	-	0.12	**0.92**	-	0.15	**0.75**
Phe	-	0.46	**0.78**	-	0.05	**0.91**
Ant	-	**0.53**	0.19	-	-	**0.69**
Flu	0.06	**0.95**	0.12	-	0.29	**0.91**
Pyr	0.08	**0.92**	0.28	0.15	**0.53**	**0.81**
BaA	0.27	**0.85**	-	0.36	**0.70**	-
Chr	0.33	**0.91**	-	**0.53**	**0.53**	0.09
BbF	**0.53**	**0.78**	-	**0.57**	**0.81**	0.05
BkF	**0.48**	**0.86**	-	0.39	**0.89**	-
BaP	-	**0.97**	0.07	0.37	**0.81**	0.06
IP	0.27	**0.69**	-	0.41	**0.84**	-
BghiP	**0.50**	**0.74**	0.18	0.42	**0.85**	-
$C_{14}H_{30}$	**0.91**	0.12	-	0.19	-	-
$C_{15}H_{32}$	**0.93**	0.03	-	0.18	-	-
$C_{16}H_{34}$	**0.92**	0.02	-	0.17	-	-
$C_{17}H_{36}$	**0.88**	0.01	-	0.25	-	-
$C_{18}H_{38}$	**0.87**	0.03	-	0.12	-	-
$C_{19}H_{40}$	**0.93**	0.11	-	0.26	-	-
$C_{20}H_{42}$	**0.77**	0.38	0.26	**0.66**	-	-
$C_{21}H_{44}$	**0.69**	0.47	-	**0.62**	-	-
$C_{22}H_{46}$	**0.57**	**0.54**	-	**0.52**	-	-
$C_{23}H_{48}$	**0.96**	0.04	0.01	**0.46**	0.08	-
$C_{24}H_{50}$	0.19	-	0.04	**0.44**	0.07	-
$C_{25}H_{52}$	**0.71**	-	0.07	**0.95**	0.13	-
$C_{26}H_{54}$	**0.95**	0.16	-	**0.95**	0.13	-
$C_{27}H_{56}$	**0.94**	0.2	-	**0.97**	0.09	-
$C_{28}H_{58}$	**0.97**	0.17	-	**0.97**	0.09	-
$C_{29}H_{60}$	**0.93**	0.23	-	**0.96**	0.12	-
$C_{30}H_{62}$	**0.91**	0.2	0.11	**0.94**	0.10	0.01
$C_{31}H_{64}$	**0.95**	0.23	-	**0.94**	0.10	0.00
$C_{32}H_{66}$	**0.82**	0.15	0.25	**0.94**	0.10	0.01
$C_{33}H_{68}$	**0.90**	0.02	-	**0.95**	0.08	-
explained variance %	51.7	20.6	10.5	47.2	30.7	9.9

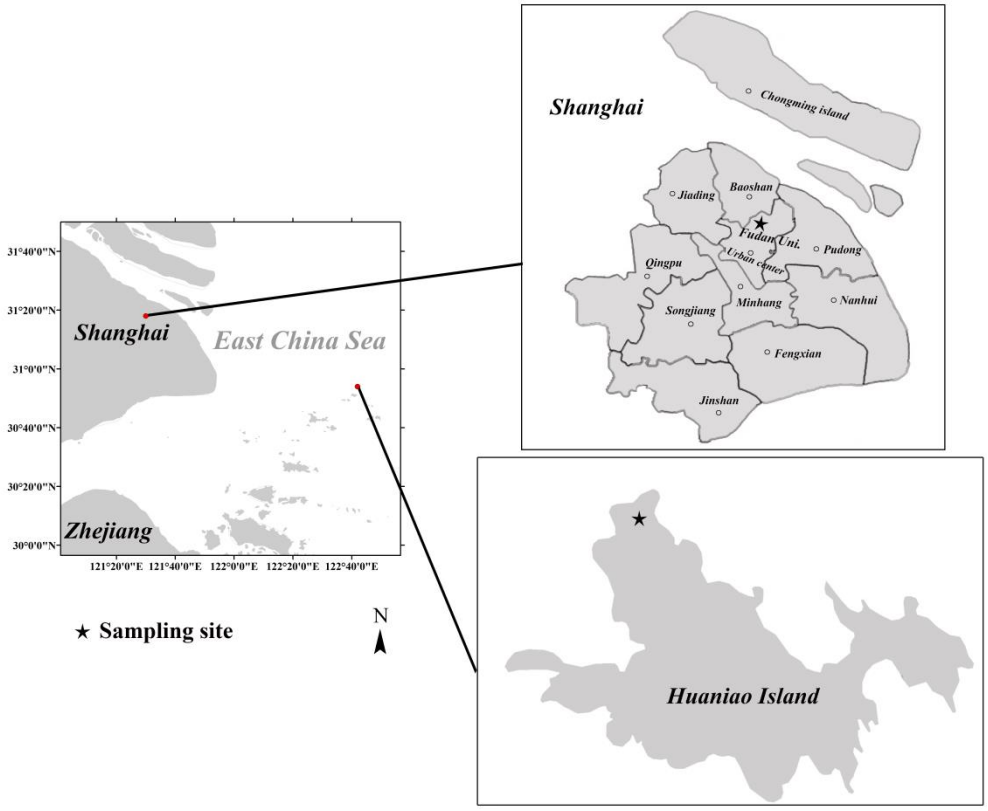

Fig. 1 Sampling sites at Shanghai and Huaniao Island (HNI).

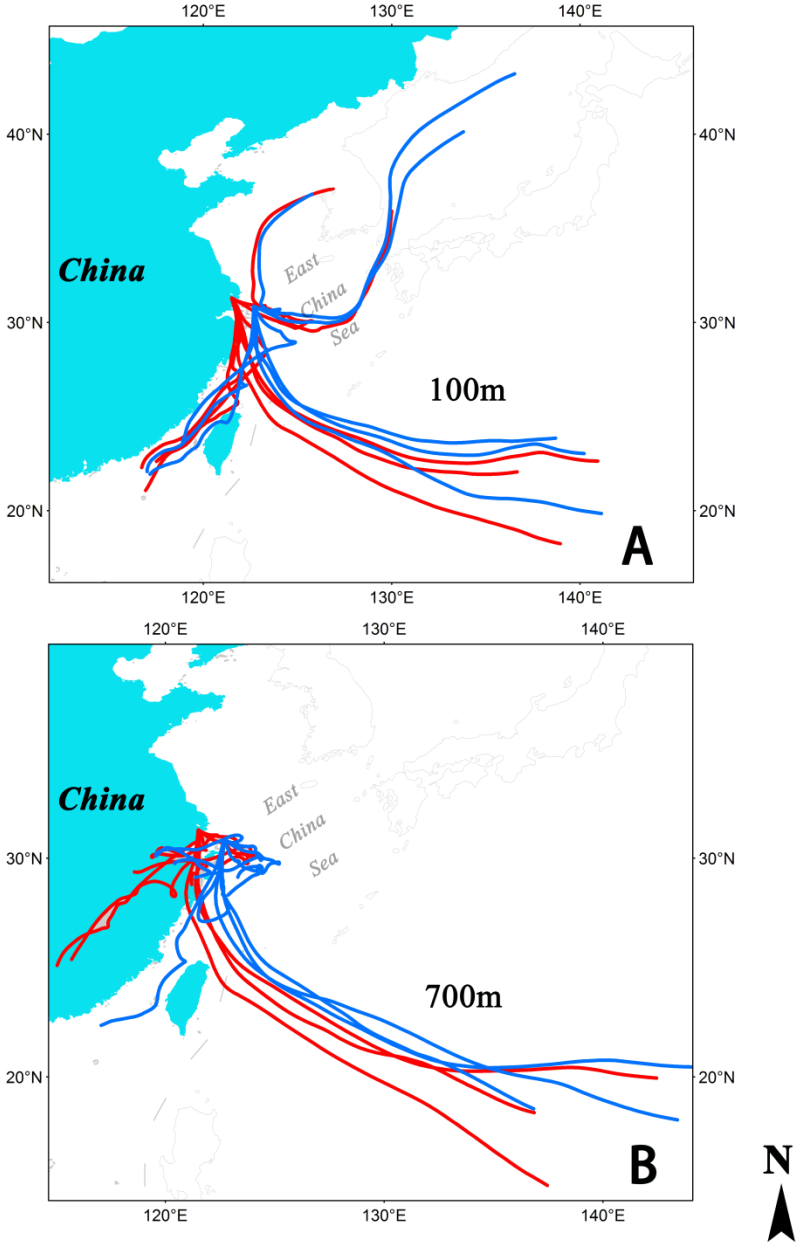

Fig. 2 3-day back trajectories from the altitudes of both 100 m and 700 m arrived at Shanghai (red line) and HNI (blue line).

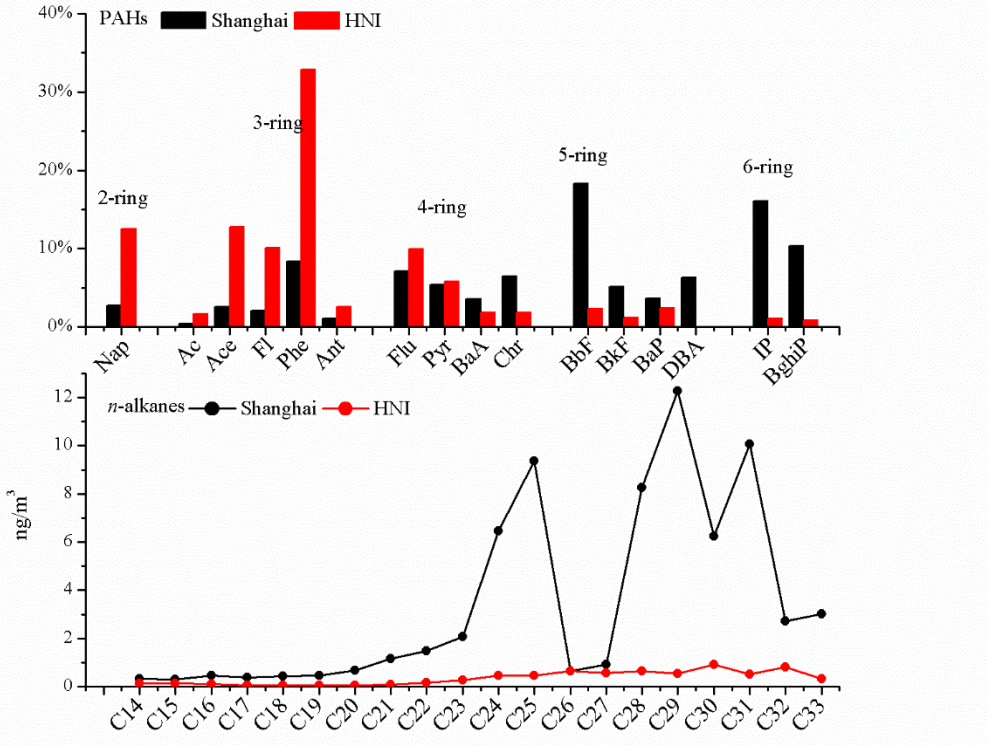

Fig. 3 The compositions of PAHs and *n*-alkanes of $PM_{2.5}$ at Shanghai and HNI.

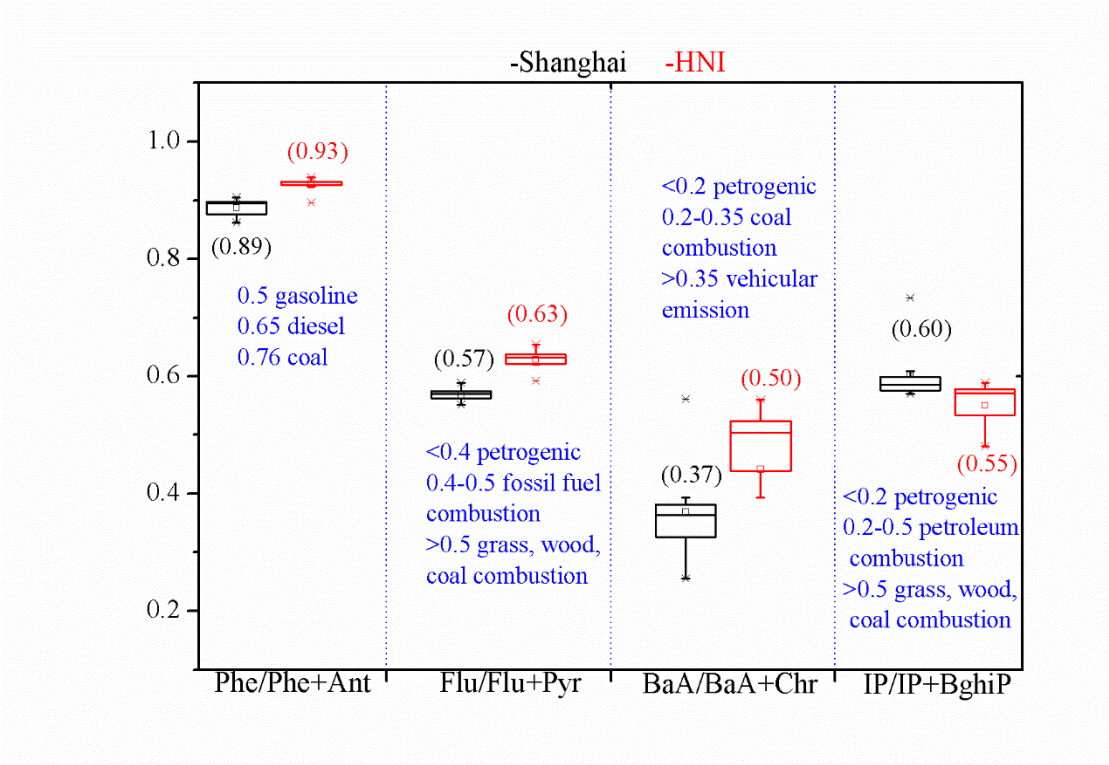

Fig.4 The diagnostic ratios of Phe/(Phe + Ant), Flu/(Flu + Pyr), BaA/(BaA + Chr) and IP/(IP + BghiP) of $PM_{2.5}$ at Shanghai and HNI.

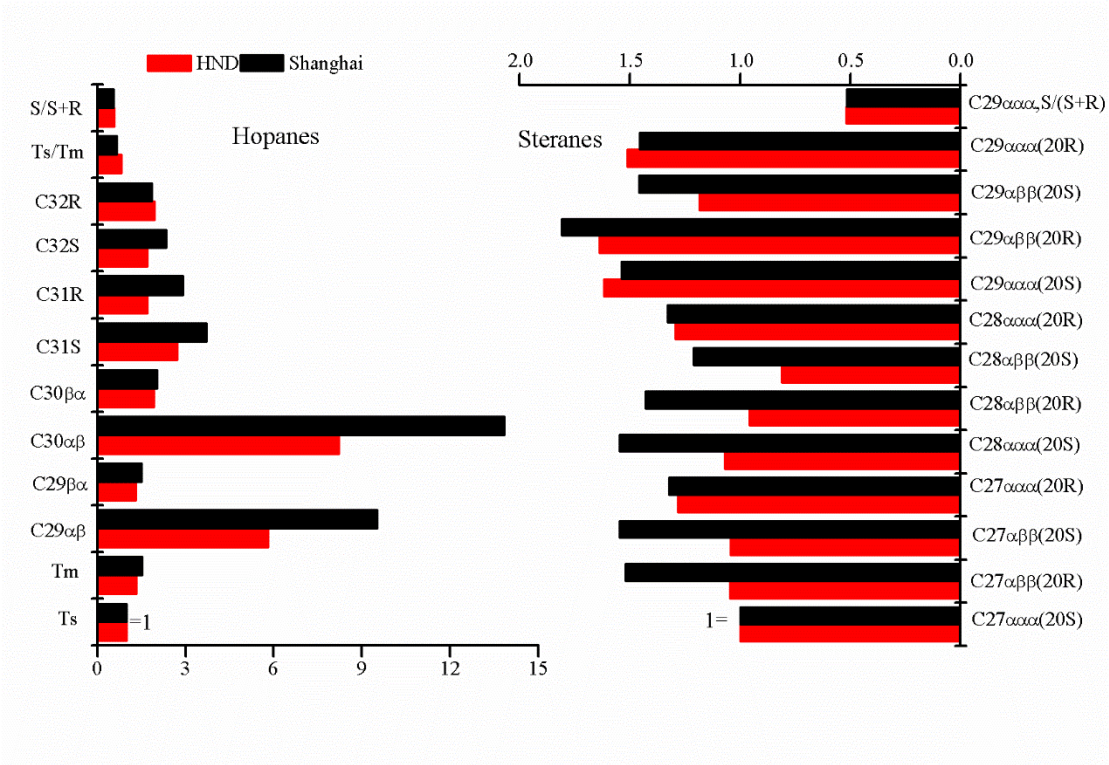

Fig.5 Distribution diagrams of relative hopane and sterane abundances of $PM_{2.5}$ at Shanghai and HNI. (Ts:18α(H)-22,29,30-trisnorneohopane;Tm:17α(H)-22,29,30-trisnorhopane;C29αβ:17α(H),21β(H)-norhopane;C29βα:17β(H),21α(H)-norhopane;C30αβ:17α(H),21β(H)-hopane;C30βα:17β(H),21α(H)-hopane;C31S:22S-17α(H),21β(H)-homohopane;C31R:22R-17α(H),21β(H)-homohopane;C32S:22S-17α(H),21β(H)-bishomohopane;C32R:22R-17α(H),21β(H)-bishomohopane)

(C27ααα(20S), C27αββ(20R), C27αββ(20S), C27ααα(20R), C28ααα(20S), C28αββ(20R), C28αββ(20S), C28ααα(20R), C29ααα(20S), C29αββ(20R), C29αββ(20S), C29ααα(20R), and ααα = 5α(H), 14α(H), 17α(H)-steranes; αββ = 5α(H), 14β(H), 17β(H)-steranes, R and S = C-20 R and S configuration, respectively.)